Imaging Microglia Surveillance during Sleep-wake Cycles in Freely Behaving Mice

Xiaochun Gu[2,3,6*#], Zhong Zhao[5,6#], Xueli Chen[6], Lifeng Zhang[6], Huaqiang Fang[6], Ting Zhao[7], Shenghong Ju[2], Weizheng Gao[4], Xiaoyu Qian[4], Xianhua Wang[1,6], Jue Zhang[4], Heping Cheng[1,6*]

1 National Biomedical Imaging Center, State Key Laboratory of Membrane Biology, Peking-Tsinghua Center for Life Sciences, College of Future Technology, Peking University, Beijing 100871, China

2 Jiangsu Key Laboratory of Molecular and Functional Imaging, Department of Radiology, Zhongda Hospital, Medical School, Southeast University, Nanjing 210009, China

3 Key Laboratory of Developmental Genes and Human Diseases, Department of Histology Embryology, Medical School, Southeast University, Nanjing 210009, China

4 Academy of Advanced Interdisciplinary Study, College of Engineering, Peking University, Beijing 100871, China

5 Institute of Basic Medical Sciences Chinese Academy of Medical Sciences, School of Basic Medicine Peking Union Medical College, Beijing 100005, China

6 Research Unit of Mitochondria in Brain Diseases, Chinese Academy of Medical Sciences, PKU-Nanjing Institute of Translational Medicine, Nanjing 211899, China

7 Nanjing Raygenitm Biotech Co., Ltd, Nanjing 211899, China

*Address correspondence to: chengp@pku.edu.cn, xiaochun.gu@seu.edu.cn

# These authors contributed equally to this work

Abstract

Microglia surveillance manifests itself as dynamic changes in cell morphology and functional remodeling in response to fluctuations in the neural environment. Whether and how microglia surveillance is coupled to brain state switches during natural sleep-wake cycles, as well as under sleep deprivation, remain unclear. To address this question, we used miniature two-photon microscopy (mTPM) to acquire time-lapse high-resolution microglia images of the somatosensory cortex, along with EEG/EMG recordings and behavioral video, in freely-behaving mice. We uncovered fast and robust brain state-dependent changes in microglia surveillance, occurring in parallel with sleep dynamics and early-onset phagocytic microglial contraction during sleep deprivation stress. With the aid of the biosensor $GRAB_{NE2m}$, we also detected local norepinephrine fluctuation occurring in a sleep state-dependent manner. We showed that the locus coeruleus-norepinephrine system, which is crucial to sleep homeostasis, is required for both sleep state-dependent and stress-induced microglial responses and β_2-adrenergic receptor signaling plays a significant role in this process. These results provide direct evidence that microglial surveillance is exquisitely tuned to signals and stressors that regulate sleep dynamics and homeostasis so as to adjust its varied roles to complement those of neurons in the brain. *In vivo* imaging with mTPM in freely behaving animals, as demonstrated here, opens a new avenue for future investigation of microglia dynamics and sleep biology in freely behaving animals.

Introduction

Sleep is a highly conserved and essential phenomenon of the brain and serves numerous cognitive as well as metabolic and immunologic functions. Moreover, the sleep-wake transition represents a specific and prominent change in the brain state (Besedovsky et al., 2019; Rasch and Born, 2013). As compared to a wakeful brain, the sleeping brain shows more synchronous neuronal activities, which can be characterized by electroencephalography (EEG). Sleep has two main stages: the non-rapid eye movement (NREM) state, which is thought to promote clearance of metabolic waste partly through increased flow of interstitial fluid (Feng et al., 2019), and the rapid eye movement (REM) state, with EEG patterns similar to wakefulness yet with muscle atonia as well as vivid dreaming in humans (Besedovsky et al., 2019). In addition, sleep, especially NREM, is directly involved in memory consolidation (Fogel and Smith, 2011; Rasch and Born, 2013). However, the underlying biological dynamics and especially the cellular mechanisms of sleep regulation are not entirely understood (Frank, 2018; Frank and Heller, 2018).

Growing evidence shows that microglia dynamics are coupled to and intertwined with the sleep-wake cycle (Deurveilher et al., 2021; Hristovska et al., 2022). Microglia are resident innate immune cells ubiquitously distributed in the central nervous system and account for 10–15% of all brain cells (Wolf et al., 2017). Microglia surveillance refers to dynamic changes in cell morphology that accompany functional remodeling in response to changes in the neural environment (Liu et al.,

2019; Nimmerjahn et al., 2005; Stowell et al., 2019). It has been shown that microglia ablation disrupts the maintenance of wakefulness and promotes NREM sleep (Corsi et al., 2022; Liu et al., 2021), while enhancing an animal's fear memory consolidation (Wang et al., 2020). Conversely, acute and chronic sleep deprivation (SD) leads to microglia activation amidst a proinflammatory state triggered by elevated circulating levels of cytokines (C-reactive protein, TNF-α, IL-1, and IL-6) (Krueger et al., 2011). Thus, it is of critical interest to explore whether microglia surveillance can sense and respond to brain state changes during both natural sleep-wake cycles as well as under SD stress.

The investigation of microglial surveillance during the sleep-wake cycle demands technologies suitable to track the rapid dynamics of natural microglia behavior in real time. Though there have been pioneering studies on microglia dynamics in cultured brain slices (Honda et al., 2001), static *ex vivo* conditions can hardly recapitulate the dynamic microenvironments and neuronal activities *in vivo*. Based on results obtained from fixed brain slices, it has been shown that chronic sleep restriction but not acute sleep loss causes microglia process changes (Bellesi et al., 2017), but it is difficult to use this approach to reconstruct the dynamic behavior of microglia accurately and quantitatively. As a major advance, two-photon microscopy has recently been applied to image microglia in head-fixed or anesthetized animals, revealing microglial process motility, chemotaxis and homeostatic translocation, and multifaceted microglia-neuron interactions *in vivo* (Davalos et al., 2005; Eyo et al., 2018; Liu et al., 2019;

91 Stowell et al., 2019). However, because of mechanical constraints or anesthetics, this
92 technology still precludes experimental paradigms in which natural sleep-wake cycle
93 is undisturbed. In this regard, the recent advent of miniaturized two-photon
94 microscopy (mTPM) has provided a powerful new tool ideal for fast and high-
95 resolution brain imaging in freely behaving rodents (Zong et al., 2021, 2017). With
96 the aid of mTPM, researchers have mapped the functional network topography of the
97 medial entorhinal cortex (Obenhaus et al., 2022), deciphered the microcircuit
98 dynamics in the dorsomedial prefrontal cortex during social competition (Zhang et al.,
99 2022), and unraveled the specific itch signal processing in the primary somatosensory
100 cortex (Chen et al., 2021).

101 In this study, we aimed to determine whether microglia surveillance undergoes
102 any significant changes during natural sleep-wake cycles, and if so, what is the
103 underlying regulatory mechanism. Using different models of mTPM tailored for high-
104 resolution, multi-plane or large field-of-view (FOV) imaging, we monitored microglia
105 in the somatosensory cortex of mice during natural sleep-wake cycles or while being
106 subjected to acute SD. We found robust sleep state-dependent and SD-induced
107 changes in microglia surveillance with characteristics differing from those induced by
108 anesthetics. Furthermore, we showed that norepinephrine signals from the axonal
109 projections of the locus coeruleus (LC) underlie the state-dependence of microglia
110 surveillance and β_2-adrenergic receptor (β_2AR) signaling plays a significant role in
111 this process.

Results

Imaging microglia dynamics in freely behaving mice

To visualize microglial morphology and dynamics during the sleep-wake cycle, microglia were specifically labeled with green fluorescent protein (GFP) expressed under the control of an endogenous Cx3cr1 promoter (Cx3cr1-GFP). Time-lapse imaging of the somatosensory cortex utilized the fast and high-resolution miniature two-photon microscope (FHIRM-TPM) recently developed by our laboratory (Zong et al., 2017), and EEG/Electromyography (EMG) signals and behavior videos were simultaneously recorded to determine corresponding sleep-wake states (Fig. 1a-c and Supplementary Fig. 1). The focal plane of the FHIRM-TPM was placed 50-100 μm beneath the surface of the somatosensory cortex with a field-of-view (FOV) of 220 × 220 μm (Fig. 1d). Under the experimental conditions, we were able to track morphological and positional changes of a cohort of 5-10 microglia at a frame rate of 5 frames per second (FPS) over prolonged durations of greater than 10 hours (Supplementary Fig. 1 and Video), while the animals were allowed to roam and behave freely and their sleep-wake cycles remained undisturbed. Though we were initially concerned with potential photoxicity associated with prolonged mTPM imaging, no changes in microglial morphology and fluorescent intensity were evident even after non-stop recording over the entire protocol period (Supplementary Fig. 1). This remarkable result indicates that photo damage is minimal, if any, during *in vivo* imaging (Supplementary Fig. 1).

133 Dynamic changes in microglial area, branching points, and process end-point
134 speed were then analyzed using Imaris software (Fig. 1 e1-e3′ and Supplementary Fig.
135 1). We found that individual microglia maintained a relatively stable territory of
136 surveillance over the entire experimental period, even while their individual
137 projections extended and contracted incessantly, giving rise to a process end point
138 motility of 1.39 ± 0.09 μm/min in the wake state (Fig. 1f-h). These results show that
139 mTPM in conjunction with multi-modal recordings of EEG/EMG and behavioral
140 videos enables *in vivo* visualization of microglia dynamics over multiple time scales
141 in freely behaving mice. Interestingly, we also observed occasional short-range
142 translocation in a few cells, suggesting the ability of microglia to survey territories
143 beyond their own boundaries, in general agreement with recent observations in head-
144 fixed mice (Eyo et al., 2018).

145

146 **Microglia surveillance during the sleep-wake cycle**

147 By simultaneously imaging microglia and recording EEG/EMG throughout a
148 sleep-wake cycle, we obtained continuous 4-6 h datasets from different mice and, in
149 conjunction with video interpretation, segmented and sorted them into subgroups
150 corresponding to wake, NREM, and REM states (Fig. 2a). For each state we
151 quantified morphological features and process motility from 15-20 cells. Wake and
152 NREM states lasting longer than 1 min were identified, for which the last 30-seconds
153 recording was selected, and REM states lasting longer than 30 seconds for the

154 characterization of possible state-dependent microglia dynamic surveillance.

155 We found that during the NREM and REM states, microglial process length and
156 surveillance area increased compared with those during wakefulness (Fig. 2b-d, b′-d′).
157 Concomitantly, the number of branching points significantly increased, while end-
158 point moving speed of microglial processes decreased (Fig. 2e-h), indicating state-
159 dependent changes in microglial morphology as well as process motility under natural
160 sleep-wake cycles. To provide a volumetric view of the dynamics of microglial
161 morphology, we adapted our latest version of mTPM with an electrical tunable lens
162 (ETL) capable of imaging variable focal planes (Fig. 2i-o and Supplementary Fig. 2)
163 (Zong et al., 2021). Multi-plane reconstruction revealed more extended process
164 lengths and greater branch point numbers as compared to single-plane imaging as
165 expected (Fig. 2l, n). The volume of surveillance for individual microglia changed
166 from 1661 ± 264.4 μm^3 in the wake state to 3802 ± 670.5 μm^3 in REM state and 4616
167 ± 324.6 μm^3 in NREM state (Fig. 2m). Similar to results obtained with single-plane
168 imaging, the end-point speed of processes decreased in REM and NREM compared to
169 the wake state (Fig. 2o). While both REM and NREM had the same trends in change
170 as compared to the wake state, significantly greater changes were associated with
171 NREM than REM in terms of cell volume, branch length, branch number, and end-
172 point speed (Fig. 2l-o). These results demonstrate differential microglial dynamic
173 surveillance as the brain state switches among wakefulness, REM and NREM, and the
174 state-dependent morphological and process-motility changes can be robustly

175 reproduced with either single-plane or volumetric imaging. Intriguingly, microglia can
176 even sense and respond to subtle differences between REM and NREM states.
177 Because more extended microglia are thought to have greater surveillance ability
178 (Kierdorf and Prinz, 2017), our results support the notion that microglia during the
179 NREM and REM periods tend to be more active in the opportune clearing of
180 metabolic wastes accumulated during the wake states.

181 To this end, it is also instructive to compare and contrast REM/NREM state-
182 dependent characteristics with those induced by anesthesia. In mice under isoflurane
183 (1.2% in air) for 20-30 min, we found that microglial length, area, number of
184 branching points (Supplementary Fig. 2) were similarly increased compared with the
185 wake state, as was the case in NREM and REM. However, the end-point movement of
186 processes exhibited opposite changes (Liu et al., 2019), increasing with anesthesia but
187 decreasing in sleep states (Fig. 2h, o and Supplementary Fig. 2). This result shows
188 that microglia surveillance appears to differ qualitatively between sleep and
189 anesthesia states.

190

191 **Acute SD promotes contraction of microglial processes**

192 Sleep loss is detrimental to brain function and results in structural plastic changes
193 in nerve cells. Whether microglia dynamic surveillance alters after sleep loss remains
194 controversial (Bellesi et al., 2017; Wang et al., 2020). Therefore, we induced acute SD

195 in mice by forcing the animals to exercise and interrupting sleep with a rotatory rod,
196 starting at 9:00 am and lasting for six hours (zeitgeber time 2-8) (Fig. 3a). The
197 duration of recovery sleep, especially NREM sleep, increased after SD
198 (Supplementary Fig. 3). In the wake state, microglia typically exhibited an extended
199 form with ramified, long, thin processes. Overt morphological changes occurred as
200 early as 3h after SD, when microglia presented a contracted form bearing short and
201 thick processes. By 6h, nearly all microglia cells were converted into a phagocytic
202 form, assuming an amoeboid shape with few processes (Fig. 3b-d). We found that
203 microglial length, area and number of branching points decreased with the continuous
204 SD (Fig. 3e-h). The same changes were observed in 3D reconstruction
205 (Supplementary Fig. 3). Changes in the end-point speed of processes appeared to be
206 biphasic, increasing at 3h SD and then declining below baseline level at 6h SD (Fig.
207 3h); the latter may result in part from the dramatic shrinkage of the processes. As the
208 sleep pressure was eased during recovery sleep, morphological changes of microglia
209 were partially reversed over a timescale of several hours (Supplementary Fig. 3). Thus,
210 our real-time recording in live animals clearly demonstrates that SD stress induces
211 microglia to assume an active state and conspicuous microglial response occurs early
212 in SD.

213

214 **NE changes in somatosensory cortex during the sleep-wake cycle**

215 Next, we sought to determine a possible signaling mechanism(s) that incites

microglia surveillance state- and stress-dependent changes. Among a number of candidates responsible for stress responses, norepinephrine (NE) has recently been shown to play a crucial role in microglia surveillance by responding to neuronal network activity (Liu et al., 2019) and partaking of synaptic plasticity (Stowell et al., 2019). Therefore, we combined mTPM imaging with EEG and EMG recording to determine whether NE levels in the somatosensory cortex fluctuate during the sleep-wake cycle to control microglia surveillance. We imaged extracellular NE dynamics in somatosensory cortical neurons with NE biosensor $GRAB_{NE2m}$ (Fig. 4a), which was developed based on G protein receptors (Feng et al., 2019; Kjaerby et al., 2022). The biosensor was expressed on the plasma membrane of neurons to report the dynamic change of the extracellular NE. Dynamic changes of NE levels was evident in the somatosensory cortex during wake, NREM and REM states (Fig. 4b). NE levels reached higher levels during longer awakenings, while the lowest NE levels were detected during REM sleep (Fig. 4b) and the largest changes in NE levels were recorded occurred during the transition from REM to wake (Fig. 4b). During NREM sleep, the NE oscillated dynamically around a relatively low level (Fig. 4b), with brief increases that might be related to memory consolidation (Kjaerby et al., 2022). On average, mean levels of NE exhibited a brain-state dependent change, varying in a decreasing order from wake to NREM and to REM (Fig. 4c). These results are in general agreement with recent observations that NE fluctuates in a sleep-state dependent manner in the medial prefrontal cortex, and suggest that NE may play a crucial role in controlling the stage dependent microglial changes.

238

239 **Role of the LC-NE signal in controlling the microglia dynamic surveillance**

240 To determine possible involvement of NE in sleep state- and SD-induced
241 microglia surveillance, we used the locus coeruleus (LC)-selective neurotoxin, N-(2-
242 chloroethyl)-n-ethyl-2-bromobenzylamine (DSP4; applied 2 days before imaging) to
243 ablate LC axons projecting into the cortex (Supplementary Fig. 4) (Del C. González et
244 al., 1998) and characterized microglial surveillance with and without an LC-NE signal
245 (Fig. 5a). DSP4 application led to a significant increase in sleep states, particularly
246 NREM sleep (Supplementary Fig. 4), in agreement with previous studies (Del C.
247 González et al., 1998). Meanwhile, the characteristics of NE dynamics in different
248 brain states were also changed by DSP4 (Supplementary Fig. 4). Importantly, the
249 sleep state-dependent changes in microglia surveillance were abolished altogether;
250 neither microglial morphology nor process motility displayed any of the previously
251 significant changes seen when the brain states cycled across wake-REM-NREM (Fig.
252 5b-g). Likewise, DSP4 treatment completely prevented SD-induced alteration of
253 microglia surveillance (Supplementary Fig. 4). These results indicate an essential role
254 for the LC-NE signal in sleep- and stress-dependent state modulation of microglia
255 surveillance.

256 The effects of the neural modulator NE are mediated by two families of G-
257 protein-coupled receptors, α and β-adrenergic receptors (ARs), each comprising
258 several subtypes and it has been shown that β_2AR stimulation rapidly induces

259 microglia dynamic surveillance (Gyoneva and Traynelis, 2013; Liu et al., 2019;
260 Stowell et al., 2019). We, therefore, examined microglia surveillance in β_2AR KO
261 animals during natural sleep-wake cycles and under SD stress. Similar to LC axon
262 ablation, β_2AR KO disturbed wake-sleep homeostasis, as manifested by a lengthening
263 of overall sleep duration (Supplementary Fig. 4). By contrast, removal of β_2ARs
264 failed to abolish dynamic changes in microglia when the brain state switched between
265 sleep and wakefulness (Fig. 5h-n). Nonetheless, the ability of microglia to subtly
266 distinguish between REM and NREM states was largely compromised (Fig. 5h-n and
267 Supplementary Fig. 4), suggesting a partial contribution of β_2AR signaling to LC-NE
268 modulation of microglia surveillance during sleep-wake cycles. Regarding microglia
269 responses to SD stress, we showed that microglial morphology and motility remained
270 unchanged during the SD protocol in β_2AR KO animals (Supplementary Fig. 4),
271 revealing a predominant role for β_2AR signaling in LC-NE modulation of microglia
272 surveillance under SD stress.

Discussion

With the development of mTPM imaging and EEG/EMG recording in freely behaving mice, we now provide direct evidence that microglia surveillance in mouse somatosensory cortex is sleep-state dependent during natural sleep-wake cycles and that microglia contract from ramified into phagocytic forms a few hours after the onset of acute SD stress. Combined with pharmacological intervention and the use of NE biosensor and genetically manipulated animals, we showed that the LC-NE pathway mediates these state-dependent changes in microglia surveillance and that β_2AR signaling is involved in various aspects of the microglial responses, extending recent reports that the same pathway underlies microglia surveillance in the context of neuronal network activity (Liu et al., 2019) and synaptic plasticity (Stowell et al., 2019).

That microglia surveillance is sleep state-dependent substantiates an intimate relationship between rapid, robust state-dependent microglia remodeling and the biology of the sleep-wake cycle (Feng et al., 2019; Frank and Heller, 2018; Xie et al., 2013). It has been shown that microglia play a central role in the removal of metabolic waste and even cell debris from the brain (Huisman et al., 2022; Márquez-Ropero et al., 2020). Our study shows that microglia in the sleeping brain have larger area and length, consistent with greater clearance ability in the sleeping state than the waking. Recently, it has been reported that, in head-fixed mice, microglial morphological complexity was decreased in NREM sleep than during wakefulness (Hristovska et al.,

294 2022). In consideration of the altered durations of both NREM and REM sleep
295 (Hristovska et al., 2022), the unnatural sleep state would lead to an increase in the
296 microarousal state, and ultimately lead to a change in the structure of the sleep state,
297 which may be the main reason for the difference in microglia behavior from our
298 natural sleep. Furthermore, our results show that microglia surveillance significantly
299 differs between REM and NREM sleep in the somatosensory cortex, likely reflecting
300 metabolic and functional differences between the two states. More specifically,
301 previous reports have proposed differential roles between the NREM and REM sleep
302 for consolidation of different types of memories. For example, NREM sleep
303 contributes to declarative memories, whereas REM sleep is important for procedural
304 and emotional memories (Besedovsky et al., 2019; Rasch and Born, 2013). Memory
305 consolidation is closely related to synaptic plasticity, in which microglia play a very
306 important role (Corsi et al., 2022; Tuan and Lee, 2019). In this regard, our findings
307 hint at the possibility that not all features of microglia-neuron interactions, including
308 mode of action and localization, are equal in the consolidation of different types of
309 memory.

310 It has been shown that a large proportion of Iba1-immunoreactive microglia with
311 larger cell bodies and less ramified processes appear in hippocampal brain slices
312 following 48-72h of sleep deprivation and in the frontal cortex after 4.5 days of
313 chronic sleep restriction, whereas acute sleep deprivation for 8 hours had no effect on
314 microglial morphology (Bellesi et al., 2017; Hall et al., 2020). However, these

315 findings have mostly been derived from slice staining. While the present work support
316 the general conclusion that microglia surveillance is responsive to SD stress, our real-
317 time mTPM imaging *in vivo* also unmasked a progressive change in microglia
318 surveillance that occurred as early as 3h after onset of SD and full conversion of
319 microglia into the phagocytic form after 6h SD stress. This apparent disparity between
320 the current and previous reports might reflect the complications arising from *ex vivo*
321 sample preparation, because microglia surveillance is highly dynamic and sensitive to
322 neural environmental changes, evidenced by its cyclic changes during the sleep-wake
323 switch.

324 We have provided two lines of evidence that the LC-NE-β_2AR axis is involved in
325 microglial surveillance both during natural sleep-wake cycle and under SD stress.
326 Ablation of LC-NE neuronal projection abolished and knockout of β_2ARs markedly
327 altered the manifestation of the state-dependence of microglia surveillance, while the
328 latter recapitulated most, but not all, the phenotypes of the former. These findings are
329 well supported by emerging evidence that NE is necessary for microglial activation
330 (Bellesi et al., 2016; Berridge et al., 2012). First, NE is known to be a key
331 neurotransmitter that regulates sleep dynamics (Wang et al., 2020) and the dynamics
332 of microglia (Liu et al., 2019; Sugama et al., 2019). Second, it has been shown β_2AR
333 expressed at higher level in microglia than other CNS cell types (Zhang et al., 2014)
334 and microglia dynamic surveillance rapidly responds to β_2AR stimulation (Gyoneva
335 and Traynelis, 2013; Liu et al., 2019; Stowell et al., 2019). Moreover, the morphology

336 of microglia in somatosensory cortex is also regulated by neuronal activity, in a
337 microglial β_2AR-dependent manner (Liu et al., 2019). Our results also extend the
338 classic view of NE regulation of sleep and wakefulness by revealing a prominent
339 microglial component in the NE response. It should be noted that pan-tissue β_2AR
340 knockout animal model was used in the current study and it warrants future
341 investigation to pinpoint specific roles of microglial β_2AR in the brain-state dependent
342 microglial responses.

343 In addition to NE, other potential modulators also present dynamic during sleep-
344 wake cycle and may partake in the regulation of microglia dynamic surveillance. It
345 has been reported that LC firing stops (Aston-Jones et al., 1981; Rasmussen et al.,
346 1986), while inhibitory neurons, such as PV neurons and VIP neurons, become
347 relatively active during REM sleep (Brécier et al., 2022). ATP level in basal forebrain
348 is shown to be higher in REM sleep than NREM sleep (Peng et al., 2023). Similarly,
349 adenosine level in the somatosensory cortex during REM sleep is higher than in
350 NREM sleep (Response figure 1). These considerations may explain the finding that
351 β_2AR knockout failed to abolish microglial responses to sleep state switch and SD
352 stress altogether. A more complete understanding of the regulatory mechanisms of
353 microglia surveillance will help to delineate more precisely roles of microglia in
354 physiology and under stress.

355 In summary, by real-time *in vivo* mTPM imaging of microglia surveillance, we
356 uncovered the state-dependence of microglia surveillance during natural sleep-wake

357 cycles and a robust, early-onset response to SD stress. Both types of microglial
358 dynamics are under the regulation of LC-NE with the involvement of β_2ARs as one of
359 its main effectors. These results highlight that microglia undergo rapid and robust
360 remodeling of both morphology and function to fulfill multimodal roles
361 complementary to those of neurons in the brain. In addition, the methodologies
362 established in the present study may prove to be of broad application for future
363 investigations of microglia dynamics and sleep biology in freely behaving animals.

364

365 **Acknowledgements**

366 We thank Dr. Wei Xie from Southeast University and Dr. Hailan Hu from Zhejiang
367 University for their carefully reading and valuable comments; L. Wang and T. Zhu
368 from Raygenitm Biotech Co., Ltd, and Y. Guo from the company Transcend
369 Vivoscope for comments on the optics, biological experiments, and data processing;
370 and the Nanjing Brain Observatory for data processing services. The work was
371 supported by grants from the National Science and Technology Innovation 2030
372 Major Program 2021ZD0202200 and the National Natural Science Foundation of
373 China (81925022, 61975002, 31830036, 31821091, 8182780030 and 61821002), and
374 CAMS Innovation Fund for Medical Sciences (2019-I2M-5-054).

375

376 **Author contributions**

X.G. and H.C. conceived the project and supervised the research; X.G. designed and supervised the biological experiments. X.G., Z.Z. and X.C. performed the experiments and led data analysis and figure-making; X.Q. and W.G. contributed data analysis under the supervision of H.C., J.Z., and X.G; X.G. and H.C. wrote the manuscript with inputs from L.Z. and H.F., while all authors participated in discussions and data interpretation.

Competing interests

The authors declare no competing interests.

Methods

Animals

All experimental protocols were carried out with the approval of the Institutional Animal Care and Use Committee of PKU-Nanjing Institute of Translational Medicine (Approval ID: IACUC-2021-023). Male mice, 2-3 months of age, were used in accordance with institutional guidelines. Cx3cr1-GFP (Jax, #021160) heterozygous mice were used to visualize microglia with miniature two-photon microscopy (mTPM). To ablate LC-NE neurons, DSP4 (Sigma, #C8417) solution was administered intraperitoneally (50 mg/kg) twice at 24-h intervals and a minimum of 48 h before mTPM imaging. Adrb2 KO (Jax, #031496) mice were crossed with

397 Cx3cr1-GFP mice to generate (Cx3cr1-GFP+/-; Adrb2-/-) mice, which were used in
398 experiments with β_2-adrenergic receptor knock-out. Mice were housed with a standard
399 12h light/12h dark cycle and fed standard chow *ad libitum*.

400 **Surgery and electrode implantation**

401 All surgical procedures were done sterilely, and all animal-administered reagents were
402 sterile. Mice were anesthetized with isoflurane (1.5% in air at a flow rate of 0.4 L/min)
403 and maintained on a 37°C heating pad during surgery. The cerebral cortical region to
404 be imaged was localized based on the stereotactic coordinates (somatosensory area,
405 from bregma: anteroposterior, -1 mm, mediolateral, +2 mm) and marked with a fine
406 black dot. The skull over the region of interest was thinned with a high-speed micro-
407 drill under a dissection microscope. Drilling and application of normal saline were
408 done intermittently to avoid overheating and hurting the underlying cerebral tissue.
409 After removing the external layer of the compact bone and most of the spongy bone
410 layer with the drill, the area continued to thinned until an expanded smooth area (~3
411 mm in diameter) was achieved, making sure the middle was thin enough to get high
412 quality imaging. A drop of saline was applied and a 3-mm-diameter glass coverslip
413 previously sterilized in 70% ethanol was placed on this window, then dental cement
414 was applied around the glass coverslip. The mice were used in the experiment after 4
415 weeks of postoperative recovery.

416 500 nL of AAV9-hSyn-GRAB$_{NE2m}$ (BrainVTA, #PT-2393) were injected into the
417 somatosensory cortex (A/P, -1 mm; M/L, +2 mm; D/V, -0.3mm) at a rate of 50 nL/min.

418 3-mm-diameter glass coverslip were implanted and fixed on the somatosensory cortex.
419 The mice were used in the experiment one month after postoperative recovery.

420 Epidural screw electrodes (diameter 0.8 mm) were implanted bilaterally on the
421 opposite sides of the imaging window for constant EEG recording from the frontal
422 (bregma: anteroposterior, +1.5 mm, mediolateral, +1.5 mm) and parietal cortex
423 (anteroposterior, -2 mm; mediolateral, +2.5 mm). Electrodes were fixed to the skull
424 with dental cement. Another pair of electrodes was inserted into the neck muscles for
425 EMG recording. Then, a headpiece baseplate was attached to the skull with
426 cyanoacrylate and reinforced with dental cement.

427 **Simultaneous imaging and recording**

428 After recovery from surgery, mice with a clear cranial window and typical EEG/EMG
429 signals were selected for further experiments. With the mice head-fixed on the
430 imaging stage, an mTPM imaging stack was first acquired using an mTPM
431 (Transcend Vivoscope), and a proper field-of-view (FOV) with 5-10 microglial
432 somata was located 50-100 μm beneath the pial surface. The holder of the mTPM was
433 then sealed onto the baseplate over the coverslip on the head, and the mTPM could be
434 repetitively mounted and dismounted to track the same population of microglia over
435 different days (Supplementary Fig. 1).

436 Three models of mTPM were used for different experiments: FHIRM-TPM high-
437 resolution model (Zong et al., 2017) with lens NA of 0.7 and FOV of 220 × 220 μm

438 for Figs. 1-5; headpiece weight was 2.13 g, and lateral and axial resolutions were 0.74
439 and 6.53 μm, respectively. FHIRM-TPM large FOV model (Zong et al., 2021) with a
440 headpiece weight of 2.45 g, lens NA of 0.5, and FOV of 420 × 420 μm for
441 Supplementary Fig. 4, and lateral and axial resolutions were 1.13 and 12.2 μm,
442 respectively; FHIRM-TPM 2.0 ETL model (Zong et al., 2021) in Supplementary Fig.
443 2, with headpiece weight of 4.3 g, Z-depth range of 45 μm, lens NA of 0.7, lateral
444 resolution of 0.74 μm, axial resolution of 6.53 μm, and FOV of 220 x 220 μm. Images
445 were acquired to visualize the microglial surveillance: time-lapse xy imaging stack at
446 a frame rate of 5 FPS or multi-plane imaging stacks (20 planes at 2 μm intervals, 5
447 frames/s). Each model of mTPM was equipped with a water-immersion miniature
448 objective and a 920 nm femtosecond fiber laser. Excitation for fluorescence imaging
449 was achieved with 150-fs laser pulses (80 MHz) at 920 nm for GFP with a power of
450 ~25 mW after the objective.

451 The EEG/EMG signals were recorded continuously and simultaneously by Vital
452 Record (Kissei Comtec system), and mouse behavior was monitored with an infrared
453 video camera. Mice were never disturbed when they were undergoing spontaneous
454 sleep-wake cycles, feeding, or drinking.

455 **Sleep deprivation**

456 Sleep deprivation (SD) was achieved by forcing the mice to move continuously
457 through power devices (Soft maze, #XR-XS108) (Pandi-Perumal et al., 2007). The
458 experimental device consisted of a computer console, a horizontal rotating rod with a

459 diameter of 46 cm and a round mouse cage of 50 cm. The rotating rod can rotate
460 horizontally randomly (3 times/min) in clockwise and counterclockwise directions
461 under the control of the computer. The mouse was placed in the cage one hour per day
462 for one week for habituation. After baseline sleep recording, mice were sleep-
463 deprived for the duration indicated in each experiment, starting at 9:00 AM and
464 lasting up to 6h into SD.

465 **Anesthesia experiment**

466 Time-lapsed image stacks acquired between 20 and 30 min after anesthesia
467 (isoflurane, 1.5% in air at a flow rate of 0.4 L/min) were used to evaluate microglial
468 dynamic surveillance under anesthetized conditions.

469

470 **Quantification and statistical analysis**

471 **EEG/EMG data analysis**

472 EEG and EMG signals were amplified and filtered as follows: EEG, high-pass filter at
473 0.1 Hz, low-pass filter at 35 Hz; and EMG, high-pass filter at 10 Hz, low-pass filter at
474 100 Hz. All signals were digitalized at 128 Hz and stored on a computer. As described
475 previously (Bellesi et al., 2013), EEG power spectra were computed by a fast Fourier
476 transform routine for 10 s epochs. Wake, nonrapid eye movement (NREM) sleep, and
477 REM sleep were manually scored off-line (SleepSign, Kissei Comtec) in 10 s epochs

478 according to standard criteria (Fogel and Smith, 2011). Epochs containing artifacts,
479 predominantly during animal movement, were excluded from spectral analysis.

480 **Microglial Morphological Analysis**

481 In order to accurately quantify microglial morphometric changes in different brain
482 states, wake and NREM states lasting longer than 1 min were chosen, among which
483 the last 30 seconds of recording was selected, in conjunction with video interpretation,
484 for further processing and analysis. Because they were of relatively short duration,
485 REM states lasting longer than 30 seconds were used for analysis.

486 Image stacks were first processed offline using ImageJ software to correct for xy
487 motion artifacts, and the time-lapse stack was aligned using the StackReg plugin. In
488 some experiments, motion artifacts due to Z-level drift was further minimized by
489 collecting multi-plane images over ±20 μm depth at 2 μm intervals and then
490 compressing them into a single xy projection to substitute for time-lapsed xy image.
491 In this case, corresponding projections were generated over a 30-seconds window to
492 substitute for time-lapsed xy images. A maximum-intensity projection (MIP) was then
493 created from the stack for morphological analysis. The criteria to select microglia for
494 analysis included a clearly identifiable soma and processes seen in the x-y plane.

495 Next, microglial morphological analysis was done using Imaris 9.5 software and
496 the Filament module (Supplementary Fig. 1). The filament created in Imaris is a
497 connected graph-based object consisting of vertices that are connected by edges.

Feature extraction by the Filament module yielded microglial features and parameters defined as the following:

Microglial process: Same a filament dendrite in module. Microglial processes form the main structure of the filament object. Processes extend from the microglial cell body and can undergo branching. A process graph is a sequence of vertices connected by edges.

Number of branch points: Same a filament branch depth in module. The process graph is a tree-based structure that has a root point. Branching depth is defined as the number of branches or bifurcations in the shortest path from the beginning point to a given point in the process graph.

Process length: Same a filament dendrite length in module, in reference to the sum of all process lengths within the entire microglial cell.

Microglial surveillance area: Same a filament dendrite area in module, in reference to the sum of all process areas within the entire microglial cell.

Microglial surveillance volume: Same as filament dendrite volume. In volumetric imaging, it is the sum of the volumes of all processes within the microglial cell.

Process end-point speed: Same as filament track speed. The speed is calculated using the "Track over time" function and given by the absolute track length change, whether extension or retraction, divided by the corresponding elapsed time.

518 **NE signals analysis**

519 To analyze NE signals data, we binned the raw data into 1 Hz and subtracted the
520 background autofluorescence. $\Delta F/F_0$ were calculated by using the fluorescence signal
521 itself. F_0 was defined as the mean value of the lowest fluorescence signal for each 60-
522 second window in each recorded fluorescence signal. The z-score transformed $\Delta F/F_0$
523 was used for analysis. In order to accurately quantify the changes of NE signals in
524 different brain states, wake and NREM states with a duration of more than 1 min were
525 selected, in which the mean value of 30 seconds fluorescence signal at the end was
526 selected as the NE signal in this state, which was further processed and analyzed
527 combined with video interpretation. Since the duration of REM state is relatively
528 short and it enters a low level at the end of REM, the mean value of fluorescence
529 signal in the 30s before the transition from REM state to wake state is used to
530 represent NE signal in REM state.

531 **Statistical analyses**

532 Significance levels indicated are as follows: $^{*}P < 0.05$, $^{**}P < 0.01$, $^{***}P < 0.001$. All
533 data are presented as mean±SEM. All statistical tests used were two-tailed. Statistical
534 significance was determined using both parametric (ANOVA) and non-parametric
535 (Friedman) tests with post-hoc. All statistical testing was performed using GraphPad
536 Prism 6.0 (GraphPad Software). No statistical methods were used to predetermine
537 sample sizes, but our sample sizes were similar to those reported in previous
538 publications (Davalos et al., 2005; Nimmerjahn et al., 2005).

References

Aston-Jones G, Bloom FE. 1981. Activity of norepinephrine-containing locus coeruleus neurons in behaving rats anticipates fluctuations in the sleep-waking cycle. *J Neurosci* **1**:876–886. doi:10.1523/JNEUROSCI.01-08-00876

Bellesi M, De Vivo L, Chini M, Gilli F, Tononi G, Cirelli C. 2017. Sleep loss promotes astrocytic phagocytosis and microglial activation in mouse cerebral cortex. *J Neurosci* **37**:5263–5273. doi:10.1523/JNEUROSCI.3981-16.2017

Bellesi M, Pfister-Genskow M, Maret S, Keles S, Tononi G, Cirelli C. 2013. Effects of sleep and wake on oligodendrocytes and their precursors. *J Neurosci* **33**:14288–14300. doi:10.1523/JNEUROSCI.5102-12.2013

Bellesi M, Tononi G, Cirelli C, Serra PA. 2016. Region-specific dissociation between cortical noradrenaline levels and the sleep/wake cycle. *Sleep* **39**:143–154. doi:10.5665/sleep.5336

Berridge CW, Schmeichel BE, España RA. 2012. Noradrenergic modulation of wakefulness/arousal. *Sleep Medicine Reviews* **16**:187–197. doi:10.1016/j.smrv.2011.12.003

Besedovsky L, Lange T, Haack M. 2019. The sleep-immune crosstalk in health and disease. *Physiological Reviews* **99**:1325–1380. doi:10.1152/physrev.00010.2018

Brécier A, Borel M, Urbain N, Gentet LJ. 2022. Vigilance and behavioral state-dependent modulation of cortical neuronal activity throughout the sleep/wake cycle. *J Neurosci* **42**:4852–66. doi: 10.1523/JNEUROSCI.1400-21.2022

Chen X-J, Liu Y-H, Xu N-L, Sun Y-G. 2021. Multiplexed representation of itch and mechanical and thermal sensation in the primary somatosensory cortex. *J Neurosci* **41**:10330–10340. doi:10.1523/JNEUROSCI.1445-21.2021

Corsi G, Picard K, di Castro MA, Garofalo S, Tucci F, Chece G, del Percio C, Golia MT, Raspa M, Scavizzi F, Decoeur F, Lauro C, Rigamonti M, Iannello F, Ragozzino DA, Russo E, Bernardini G, Nadjar A, Tremblay ME, Babiloni C, Maggi L, Limatola C. 2022. Microglia modulate hippocampal synaptic transmission and sleep duration along the light/dark cycle. *Glia* **70**:89–105. doi:10.1002/glia.24090

Davalos D, Grutzendler J, Yang G, Kim JV, Zuo Y, Jung S, Littman DR, Dustin ML, Gan W-B. 2005. ATP mediates rapid microglial response to local brain injury in vivo. *Nat Neurosci* **8**:752–758. doi:10.1038/nn1472

Del C. González MM, Debilly G, Valatx J-L. 1998. Noradrenaline neurotoxin DSP-4 effects on sleep and brain temperature in the rat. *Neuroscience Letters* **248**:93–96.

doi:10.1016/S0304-3940(98)00333-4

Deurveilher S, Golovin T, Hall S, Semba K. 2021. Microglia dynamics in sleep/wake states and in response to sleep loss. *Neurochem Int* **143**:104944. doi:10.1016/j.neuint.2020.104944

Dworak M, McCarley RW, Kim T, Kalinchuk AV, Basheer R. 2010. Sleep and brain energy levels: ATP changes during sleep. *J Neurosci* **30**:9007–9016. doi:10.1523/JNEUROSCI.1423-10.2010

Eyo UB, Mo M, Yi M-H, Murugan M, Liu J, Yarlagadda R, Margolis DJ, Xu P, Wu L-J. 2018. P2Y12R-dependent translocation mechanisms gate the changing microglial landscape. *Cell Reports* **23**:959–966. doi:10.1016/j.celrep.2018.04.001

Feng J, Zhang C, Lischinsky JE, Jing M, Zhou J, Wang H, Zhang Y, Dong A, Wu Z, Wu H, Chen W, Zhang P, Zou J, Hires SA, Zhu JJ, Cui G, Lin D, Du J, Li Y. 2019. A genetically encoded fluorescent sensor for rapid and specific in vivo detection of norepinephrine. *Neuron* **102**:745-761.e8. doi:10.1016/j.neuron.2019.02.037

Fogel SM, Smith CT. 2011. The function of the sleep spindle: a physiological index of intelligence and a mechanism for sleep-dependent memory consolidation. *Neuroscience & Biobehavioral Reviews* **35**:1154–1165. doi:10.1016/j.neubiorev.2010.12.003

Frank MG. 2018. The role of glia in sleep regulation and function In: Landolt H-P, Dijk D-J, editors. Sleep-Wake Neurobiology and Pharmacology, Handbook of Experimental Pharmacology. Cham: Springer International Publishing. pp. 83–96. doi:10.1007/164_2017_87

Frank MG, Heller HC. 2018. The function(s) of sleep In: Landolt H-P, Dijk D-J, editors. Sleep-Wake Neurobiology and Pharmacology, Handbook of Experimental Pharmacology. Cham: Springer International Publishing. pp. 3–34. doi:10.1007/164_2018_140

Gyoneva S, Traynelis SF. 2013. Norepinephrine Modulates the Motility of Resting and Activated Microglia via Different Adrenergic Receptors. *Journal of Biological Chemistry* **288**:15291–15302. doi:10.1074/jbc.M113.458901

Hall S, Deurveilher S, Robertson GS, Semba K. 2020. Homeostatic state of microglia in a rat model of chronic sleep restriction. *Sleep* **43**:zsaa108. doi:10.1093/sleep/zsaa108

Honda S, Sasaki Y, Ohsawa K, Imai Y, Nakamura Y, Inoue K, Kohsaka S. 2001. Extracellular ATP or ADP induce chemotaxis of cultured microglia through $G_{i/o}$-coupled P2Y receptors. *J Neurosci* **21**:1975–1982. doi:10.1523/JNEUROSCI.21-

06-01975.2001

Hristovska I, Robert M, Combet K, Honnorat J, Comte J-C, Pascual O. 2022. Sleep decreases neuronal activity control of microglial dynamics in mice. *Nat Commun* **13**:6273. doi:10.1038/s41467-022-34035-9

Huisman Y, Uphoff K, Berger M, Dobrindt U, Schelhaas M, Zobel T, Bussmann J, Van Impel A, Schulte-Merker S. 2022. Meningeal lymphatic endothelial cells fulfill scavenger endothelial cell function and cooperate with microglia in waste removal from the brain. *Glia* **70**:35–49. doi:10.1002/glia.24081

Kierdorf K, Prinz M. 2017. Microglia in steady state. *Journal of Clinical Investigation* **127**:3201–3209. doi:10.1172/JCI90602

Kjaerby C, Andersen M, Hauglund N, Untiet V, Dall C, Sigurdsson B, Ding F, Feng J, Li Y, Weikop P, Hirase H, Nedergaard M. 2022. Memory-enhancing properties of sleep depend on the oscillatory amplitude of norepinephrine. *Nat Neurosci* **25**:1059–1070. doi:10.1038/s41593-022-01102-9

Krueger JM, Majde JA, Rector DM. 2011. Cytokines in immune function and sleep regulation. Handbook of Clinical Neurology. Elsevier. pp. 229–240. doi:10.1016/B978-0-444-52006-7.00015-0

Liu H, Wang X, Chen Lu, Chen Liang, Tsirka SE, Ge S, Xiong Q. 2021. Microglia modulate stable wakefulness via the thalamic reticular nucleus in mice. *Nat Commun* **12**:4646. doi:10.1038/s41467-021-24915-x

Liu YU, Ying Y, Li Y, Eyo UB, Chen T, Zheng J, Umpierre AD, Zhu J, Bosco DB, Dong H, Wu L-J. 2019. Neuronal network activity controls microglial process surveillance in awake mice via norepinephrine signaling. *Nat Neurosci* **22**:1771–1781. doi:10.1038/s41593-019-0511-3

Márquez-Ropero M, Benito E, Plaza-Zabala A, Sierra A. 2020. Microglial corpse clearance: lessons from macrophages. *Front Immunol* **11**:506. doi:10.3389/fimmu.2020.00506

Mori K, Ozaki E, Zhang B, Yang L, Yokoyama A, Takeda I, Maeda N, Sakanaka M, Tanaka J. 2002. Effects of norepinephrine on rat cultured microglial cells that express α1, α2, β1 and β2 adrenergic receptors. *Neuropharmacology* **43**:1026–1034. doi:10.1016/S0028-3908(02)00211-3

Nimmerjahn A, Kirchhoff F, Helmchen F. 2005. Resting microglial cells are highly dynamic surveillants of brain parenchyma in vivo. *Science* **308**:1314-8. doi:10.1126/science.1110647

Obenhaus HA, Zong W, Jacobsen RI, Rose T, Donato F, Chen L, Cheng H,

Bonhoeffer T, Moser M-B, Moser EI. 2022. Functional network topography of the medial entorhinal cortex. *Proc Natl Acad Sci USA* **119**:e2121655119. doi:10.1073/pnas.2121655119

Pandi-Perumal SR, Cardinali DP, Chrousos GP. 2007. Neuroimmunology of sleep. New York, NY: Springer.

Peng W, Liu X, Ma G, Wu Z, Wang Z, Fei X, Qin M, Wang L, Li Y, Zhang S, Xu M. 2023. Adenosine-independent regulation of the sleep–wake cycle by astrocyte activity. *Cell Discov* **9**:16. doi:10.1038/s41421-022-00498-9

Rasch B, Born J. 2013. About sleep's role in memory. *Physiological Reviews* **93**:681–766. doi:10.1152/physrev.00032.2012

Rasmussen K, Morilak DA, Jacobs BL. 1986. Single unit activity of locus coeruleus neurons in the freely moving cat: I. During naturalistic behaviors and in response to simple and complex stimuli. *Brain Research* **371**:324–334. doi:10.1016/0006-8993(86)90370-7

Stowell RD, Sipe GO, Dawes RP, Batchelor HN, Lordy KA, Whitelaw BS, Stoessel MB, Bidlack JM, Brown E, Sur M, Majewska AK. 2019. Noradrenergic signaling in the wakeful state inhibits microglial surveillance and synaptic plasticity in the mouse visual cortex. *Nat Neurosci* **22**:1782–1792. doi:10.1038/s41593-019-0514-0

Sugama S, Takenouchi T, Hashimoto M, Ohata H, Takenaka Y, Kakinuma Y. 2019. Stress-induced microglial activation occurs through β-adrenergic receptor: noradrenaline as a key neurotransmitter in microglial activation. *J Neuroinflammation* **16**:266. doi:10.1186/s12974-019-1632-z

Tuan L-H, Lee L-J. 2019. Microglia-mediated synaptic pruning is impaired in sleep-deprived adolescent mice. *Neurobiology of Disease* **130**:104517. doi:10.1016/j.nbd.2019.104517

Wang C, Yue H, Hu Z, Shen Y, Ma J, Li J, Wang X-D, Wang Liang, Sun B, Shi P, Wang Lang, Gu Y. 2020. Microglia mediate forgetting via complement-dependent synaptic elimination. *Science* **367**:688–694. doi:10.1126/science.aaz2288

Wolf SA, Boddeke HWGM, Kettenmann H. 2017. Microglia in physiology and disease. *Annu Rev Physiol* **79**:619–643. doi:10.1146/annurev-physiol-022516-034406

Xie L, Kang H, Xu Q, Chen MJ, Liao Y, Thiyagarajan M, O'Donnell J, Christensen DJ, Nicholson C, Iliff JJ, Takano T, Deane R, Nedergaard M. 2013. Sleep drives metabolite clearance from the adult brain. *Science* **342**:373–377.

doi:10.1126/science.1241224

Zhang C, Zhu H, Ni Z, Xin Q, Zhou T, Wu R, Gao G, Gao Z, Ma H, Li H, He M, Zhang J, Cheng H, Hu H. 2022. Dynamics of a disinhibitory prefrontal microcircuit in controlling social competition. *Neuron* **110**:516-531.e6. doi:10.1016/j.neuron.2021.10.034

Zhang Y, Chen K, Sloan SA, Bennett ML, Scholze AR, O'Keeffe S, Phatnani HP, Guarnieri P, Caneda C, Ruderisch N, Deng S, Liddelow SA, Zhang C, Daneman R, Maniatis T, Barres BA, Wu JQ. 2014. An RNA-sequencing transcriptome and splicing database of glia, neurons, and vascular cells of the cerebral cortex. *J Neurosci* **34**:11929–11947. doi:10.1523/JNEUROSCI.1860-14.2014

Zong W, Wu R, Chen S, Wu J, Wang H, Zhao Z, Chen G, Tu R, Wu D, Hu Y, Xu Y, Wang Y, Duan Z, Wu H, Zhang Y, Zhang J, Wang A, Chen L, Cheng H. 2021. Miniature two-photon microscopy for enlarged field-of-view, multi-plane and long-term brain imaging. *Nat Methods* **18**:46–49. doi:10.1038/s41592-020-01024-z

Zong W, Wu R, Li M, Hu Y, Li Y, Li J, Rong H, Wu H, Xu Y, Lu Y, Jia H, Fan M, Zhou Z, Zhang Y, Wang A, Chen L, Cheng H. 2017. Fast high-resolution miniature two-photon microscopy for brain imaging in freely behaving mice. *Nat Methods* **14**:713–719. doi:10.1038/nmeth.4305

699 **Figures**

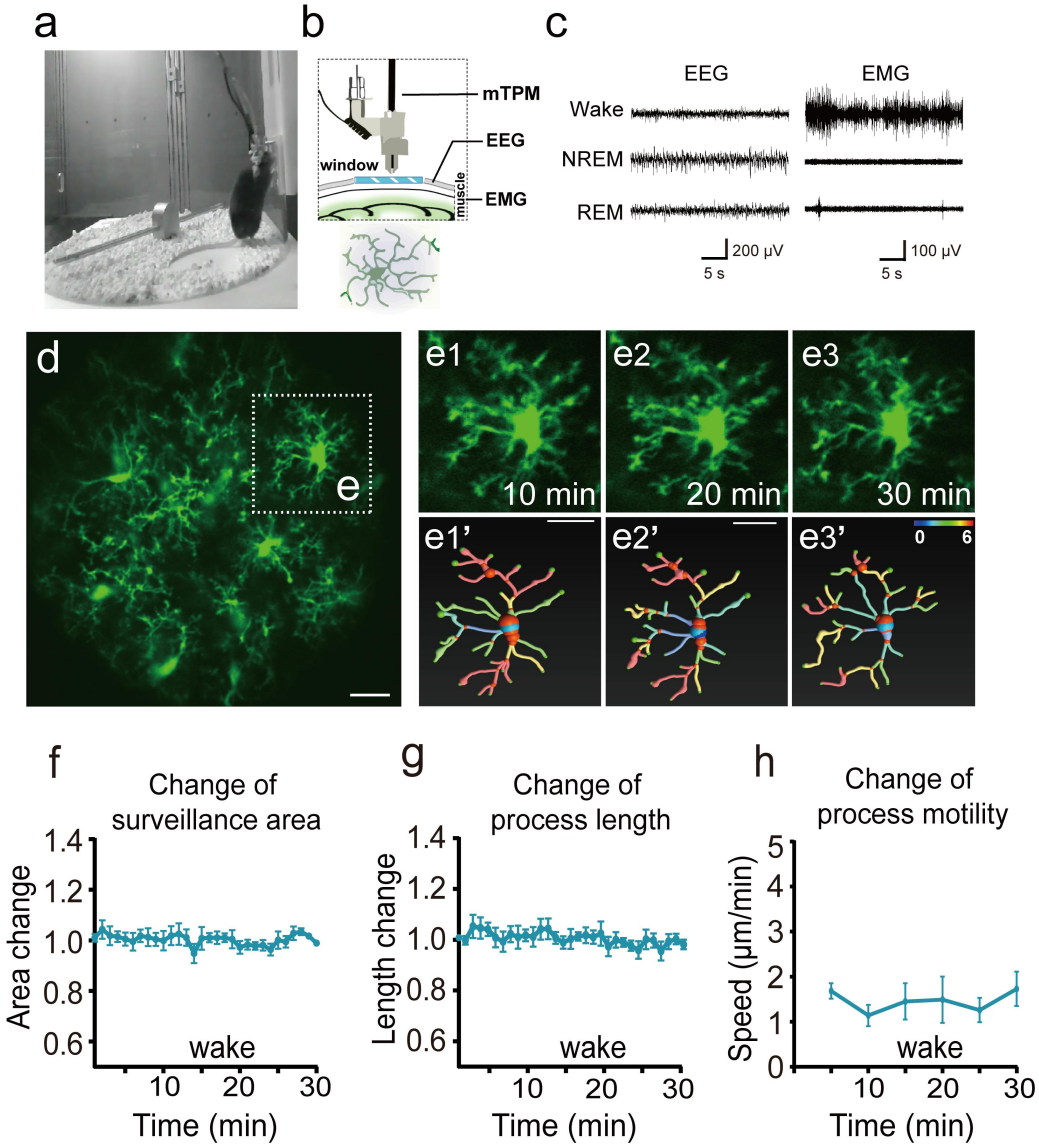

700

701 **Fig. 1. Imaging microglial surveillance in the somatosensory cortex in freely**
702 **moving mice.**

703 **(a-c)** Experimental setup. The animal was head-mounted with a miniature two-photon
704 microscope (mTPM) and EEG/EMG electrodes and behaved freely in a cylindrical
705 chamber (a). Microglia expressing GFP in the somatosensory cortex were imaged
706 through a cranial window using the mTPM (b) and the sleep/wake state of the animal
707 was simultaneously monitored using an EEG/EMG recording system (b-c).

708 **(d-e)** Microglial morphological dynamics when the animal was awake. A

representative image with a FOV of 220 × 220 μm^2. **(e1-e3)** Expanded views of selected microglia in box from (d) at 10 min (e1), 20 min (e2) and 30 min (e3) of continuous recording. **(e1'-e3')** Microglial process graphs digitally reconstruction for E1-E3 using Imaris software. In Figure e1′-e3′, the branch points of processes are represented in red and the number of different branches of the whole cell is represented as gradient colors.

(f-h) Quantitative analysis of changes in microglia surveillance area (f), process length (g), and process motility, indexed by the speed of the extension and retraction at end points of the processes (h). Note that the gross morphology of microglia remained largely unchanged over a 30-min time frame in the wake state, despite significant motility at the ends of the processes. Scale bars, 25 μm.

n = 12 cells from 3 mice. Scale bars, 30 μm. See supplementary Fig. 1-3 for more details.

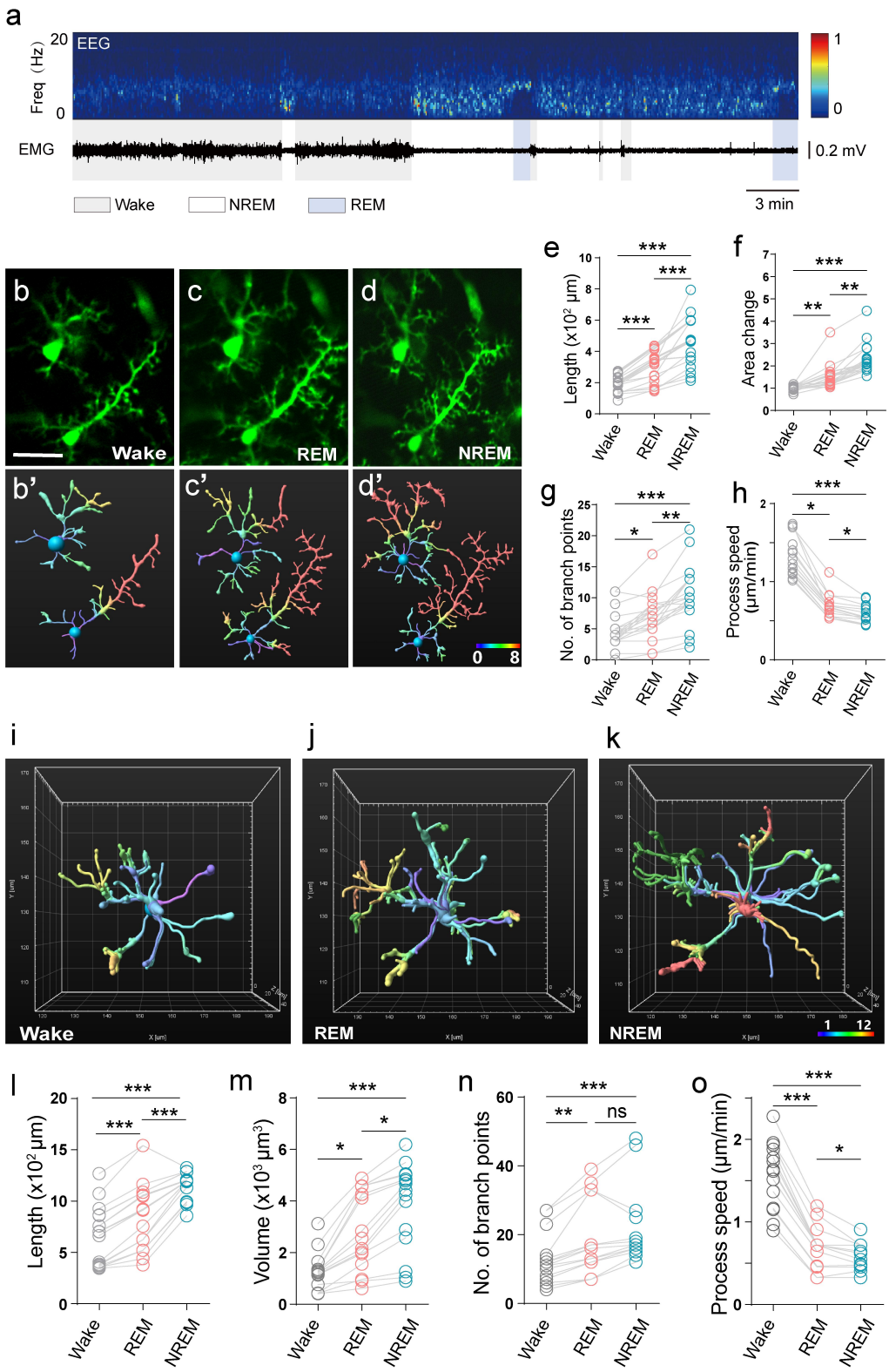

Fig. 2. Microglial surveillance is state-dependent in the sleep-wake cycle.

(a) Representative EEG/EMG recordings showing the sleep-wake stage switch. Top, EEG power spectrogram (1-20 Hz). Middle, EMG trace. Bottom, brain states classified as wake (color code: gray), REM (blue), and NREM (white).

(b-d) Representative microglial morphological changes during the sleep-wake cycle. **(b′-d′)** Microglial morphology reconstructed from b-d using Imaris software.

(e-h) Microglial morphological parameters, length (e), area change (f), number of branch points (g), and process end point speed (h), all exhibited brain state-dependent dynamic change.

One-way ANOVA with Tukey's post-hoc test in **e**; Friedman test with Dunn's post-hoc test in **f-h**; n = 20 cells from 7 mice for each group (**e-g**), n = 15 cells from 6 mice for each group (**h**); *$P < 0.05$, **$P < 0.01$, ***$P < 0.001$.

(i-o) 3D multi-plane imaging and reconstruction of microglial morphology. A 3D ETL lens was used to acquire multi-plane imaging (220*220*40 μm^3) at Z-intervals of 2 μm, at a rate of 7.5 stacks/5 min.

(i-k) 3D reconstructed microglial morphology in wake (i), REM (j), and NREM (k) states, with corresponding time stamps shown at the bottom.

(l-o) Quantitative analysis of microglial length (l), volume change (m), number of branch points (n), and process motility (o) based on multi-plane microglial imaging. Data from 3D imaging corroborated state-dependent changes of microglial morphology in the sleep-wake cycle. Scale bars, 30 μm.

One-way ANOVA with Tukey's post-hoc test in **l, o**; Friedman test with Dunn's post-hoc test in **m, n**; n = 17 cells from 7 mice for each group (**l-n**), n = 15 cells from 6 mice for each group (**o**); *$P < 0.05$, **$P < 0.01$, ***$P < 0.001$.

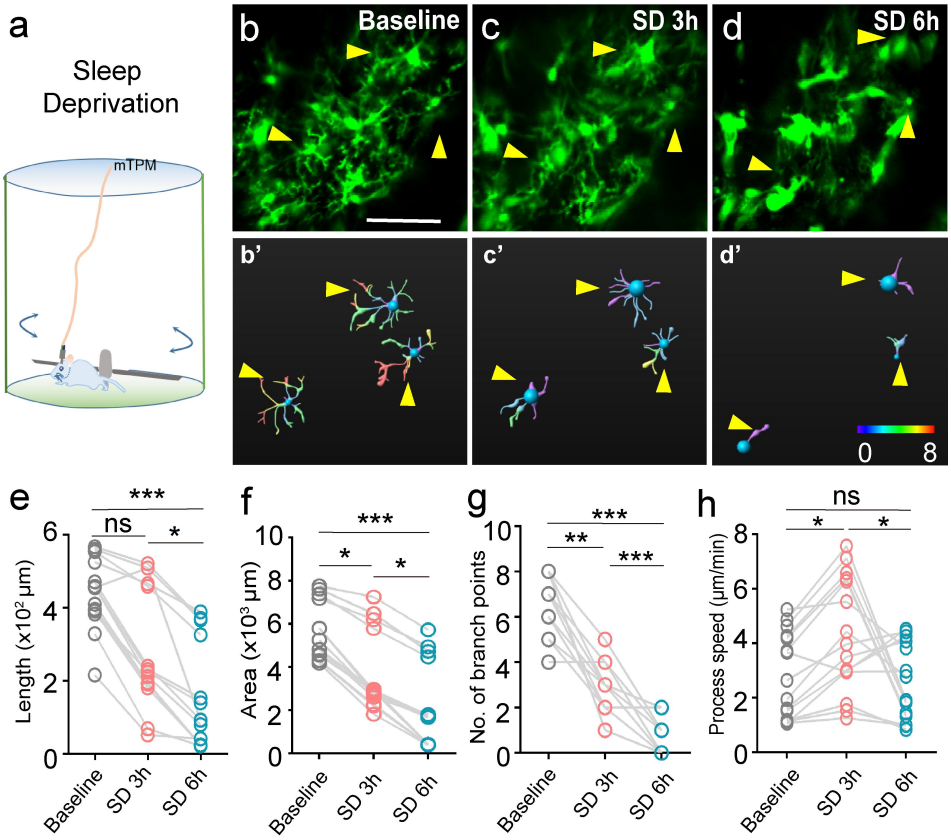

Fig. 3. Changes of microglial surveillance in the state of sleep deprivation.

(a) Experimental setup for sleep deprivation. Sleep deprivation in mice was achieved by forcing them to exercise and interrupting their sleep with the rotation of a 46-cm rod (18 turns/min) in the chamber (diameter 50 cm).

(b-d) Microglial processes contracted after sleep deprivation (SD), baseline (b), SD 3h (c), and SD 6h (d). (b′-d′) Morphological changes of microglia reconstructed using Imaris software. b'-d' correspond to b-d, respectively.

(e-h) Statistics for length (e), area (f), number of branch points (g), and process motility (h). Scale bar, 30 µm.

One-way ANOVA with Tukey's post-hoc test in **g**; Friedman test with Dunn's post-hoc test in **e, f, h**; n = 15 cells from 6 mice for each group; *$P < 0.05$, **$P < 0.01$, ***$P < 0.001$.

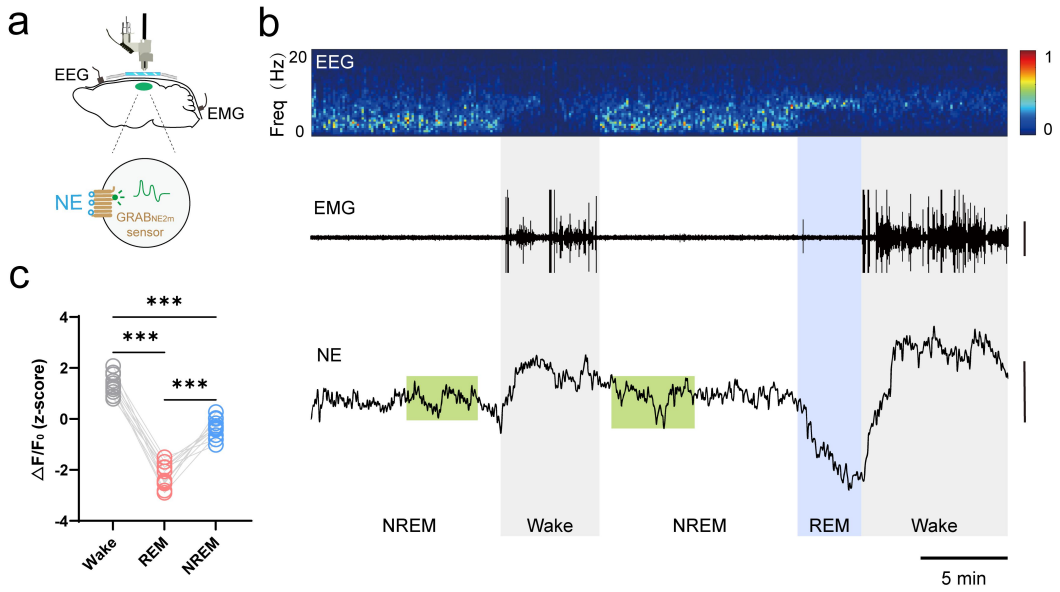

Fig. 4. NE dynamics in mouse somatosensory cortex during the sleep-wake cycle.

(a) Schematic diagram depicting mTPM recording of extracellular NE indicated by the $GRAB_{NE2m}$ sensor expressed in neurons.

(b) Representative traces of simultaneous recordings in the somatosensory cortex during the sleep-wake cycle in freely behaving mice. EEG and its power spectrogram (0-20 Hz); EMG (scale, 50 μV); NE signals reflected by the z-score of the $GRAB_{NE2m}$ fluorescence (scale, 2 z-score). The brain states are color-coded (wake, gray; NREM, white; REM, blue; NE oscillatory during NREM sleep, green).

(c) Mean extracellular NE levels in different brain states. Data from the same recording are connected by lines. ***$P < 0.001$, one-way ANOVA with Tukey's post-hoc test ($n = 11$ from 3 mice).

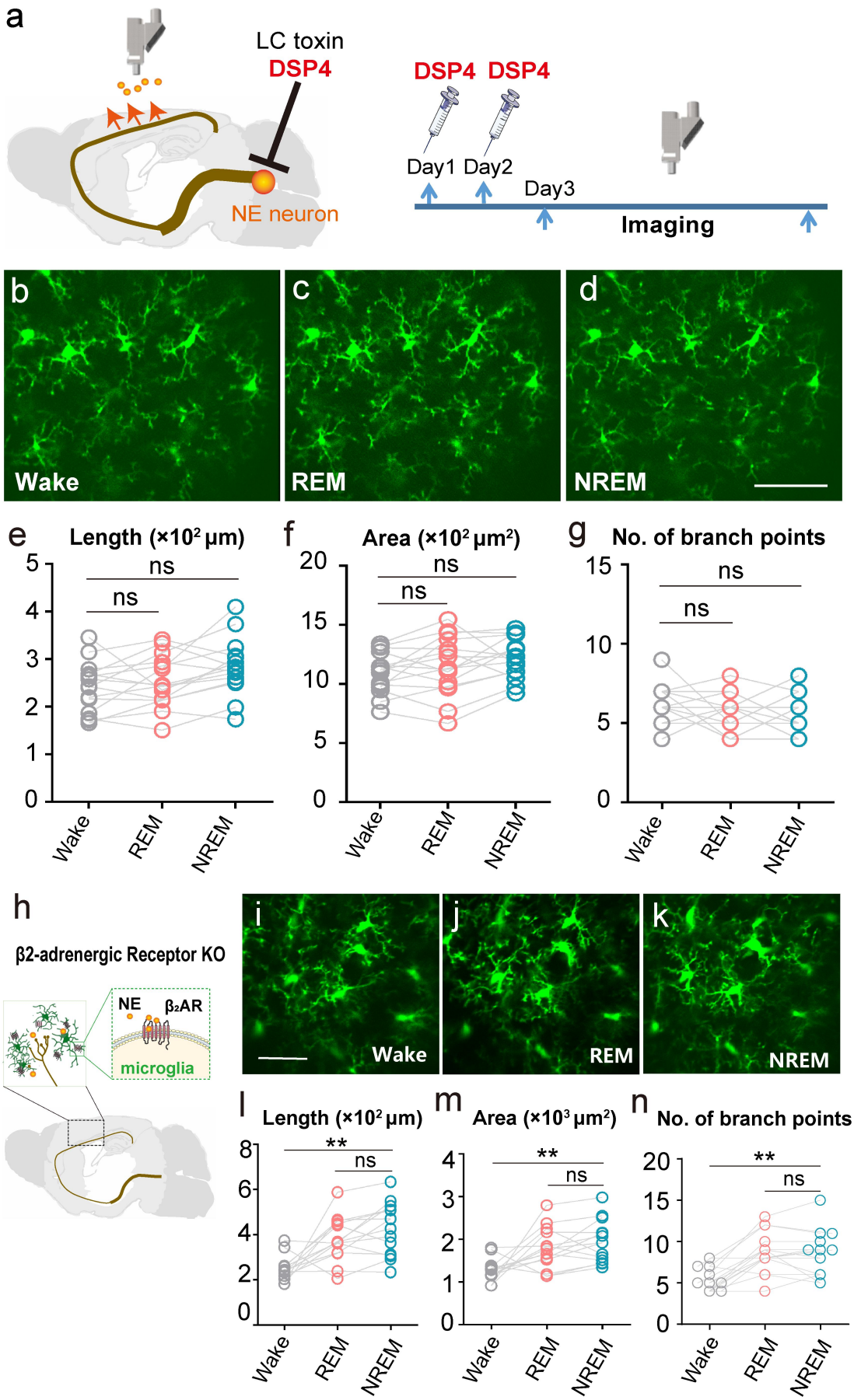
a
LC toxin
DSP4
NE neuron
DSP4 DSP4
Day1 Day2
Day3
Imaging
b
Wake
c
REM
d
NREM
e
Length (×10² μm)
ns
ns
Wake
REM
NREM
f
Area (×10² μm²)
ns
ns
Wake
REM
NREM
g
No. of branch points
ns
ns
Wake
REM
NREM
h
β2-adrenergic Receptor KO
NE
β₂AR
microglia
i
Wake
j
REM
k
NREM
l
Length (×10² μm)
**
ns
Wake
REM
NREM
m
Area (×10³ μm²)
**
ns
Wake
REM
NREM
n
No. of branch points
**
ns
Wake
REM
NREM

787

788 **Fig. 5. Microglial surveillance during natural sleep is controlled by LC-NE signal.**

789 **(a)** Experimental setup: LC-selective neurotoxin DSP4 was used to destroy LC-NE
790 neuronal axons.

791 **(b-g)** Lack of sleep/wake state-dependent microglial surveillance in LC- axon ablated
792 animals. b-d: Representative mTPM images of microglia at different states. e-g:
793 Statistics for microglial length (e), surveillance area (f), and number of branch points
794 (g) in LC-axon ablated mice.

795 One-way ANOVA with Tukey's post-hoc test in **e, f**; Friedman test with Dunn's post-
796 hoc test in **g**; n = 17 cells from 6 mice for each group; ns, not significant.

797 **(h)** Schematic diagram for β_2ARs on the plasma membrane of microglia in the
798 cerebral cortex responding to NE released from axonal terminals projected from LC.

799 **(i-k)** State-dependent microglial surveillance during sleep-wake cycle in β_2AR
800 knockout mice. Representative microglial images (i-k) and statistics for microglial
801 process length (l), surveillance area (m), and number of branch points (n) at different
802 states in (CX3CR1-GFP+/-; Adrb2-/-) mice. Scale bar, 30 μm.

803 One-way ANOVA with Tukey's post-hoc test in **m**; Friedman test with Dunn's post-
804 hoc test in **l, n**; n = 15 cells from 6 mice for each group; ns, not significant, $^{**}P <$
805 0.01.

806